IEEE Access
Multidisciplinary | Rapid Review | Open Access Journal

Received 14 March 2023, accepted 24 March 2023, date of publication 5 April 2023, date of current version 12 April 2023.

Digital Object Identifier 10.1109/ACCESS.2023.3264418

RESEARCH ARTICLE

Robust Transient Stability Emergency Control Considering Wind Power Uncertainties

YUNFEI MA, XIN WANG, GUANGCHAO GENG, (Senior Member, IEEE), AND QUANYUAN JIANG, (Senior Member, IEEE)

College of Electrical Engineering, Zhejiang University, Hangzhou 310027, China

Corresponding author: Guangchao Geng (ggc@zju.edu.cn)

This work was supported in part by the National Natural Science Foundation of China under Grant 52177120.

ABSTRACT Transient stability emergency control (TSEC) enhances power system transient stability during large disturbances but faces challenges in the high-penetration wind power grid where the wind power forecast error still cannot be ignored even with state-of-the-art forecasting methods. In this paper, the TSEC problem is modeled as robust nonlinear programming with the objective of maintaining rotor angle stability by generator tripping and load shedding while the uncertain wind power outputs are regarded as intervals. Interval programming is employed to solve the robust TSEC problem where the trajectory sensitivity analysis is applied to approximate the bounds of transient stability constraints. Numerical results on two test systems demonstrate that the proposed method improves computational efficiency and shows good performance on robustness.

INDEX TERMS Interval programming, trajectory sensitivity analysis, transient stability emergency control, wind power uncertainties, worst case.

NOMENCLATURE

The main symbols used in this paper are listed below; others are provided as required.

Abbreviations

BFGS	Broyden-Fletcher-Goldfarb-Shanno method.
DAE	Differential algebraic equations.
EEAC	Extended equal area criterion.
IO	Interval optimization.
IPM	Interior point method.
NLP	Nonlinear optimization problem.
RO	Robust optimization.
RTSEC	Robust transient stability emergency control.
SG	Synchronous generator.
SP	Stochastic programming.
SPS	Special protection scheme.
TDS	Time domain simulation.
TSEC	Transient stability emergency control.
WT	Wind turbine.

The associate editor coordinating the review of this manuscript and approving it for publication was Mouloud Denai.

Constants

H_m	Inertia constant of WT.
n_G, n_W, n_L	Number of tripped synchronous generators, tripped wind turbines and shed loads.
N_G, N_W, N_L	Number of synchronous generators, wind turbines and loads.
T_{ep}	Time constant of active power control.
T_{Ji}	Moment of inertia of the i-th generator.
T_v, k_v	Time constant and gain for the WT voltage control.
x_{qs}, x_{ds}	q-axis and d-axis reactance of WT.

Variables

i_{qs}, i_{ds}	q-axis current and d-axis current of W.T
$\boldsymbol{M}^{(1)}$	First-order disturbance factor.
P_c, Q_c	Active power and reactive power on grid side.
P_s, Q_s	Active power and reactive power on generator side.
P_W	The mechanical power extracted from the wind.
P_W^*	Optimal mechanical power of WT.

P_{Wi}^{max}, P_{Wi}^{min}	Upper and lower bound of the i-th wind power output.
T_e	Electrical torque of wind turbine.
u_G, u_L, u_W	Percentages of tripped synchronous generators, tripped wind turbines and shed loads.
V_{xi}, V_{yi}	Real and imaginary parts of voltage of i-th bus.
V_{xw}, V_{yw}	Real and imaginary parts of voltage of WT bus.
$\delta_i(t)$	Rotor angle of generator i on time t.
ω_m	Wind turbine rotor speed.
ψ_s	Magnetic flux of the permanent magnet of WT.

I. INTRODUCTION

Large-scale wind generation continues to be integrated into power systems worldwide due to environmental benefits. However, the fluctuating and uncertain nature of wind power threats power system stability and brings difficulties for power system operators [1]. For example, the wind power loss of about 1.8 GW caused Great Britain's power system blackout after successive disturbances on 9th August 2019 [2]. The power system operation condition of the high-penetration wind generation shows significant differences compared with the traditional power system, leading to higher operation requirements for power systems.

Power system emergency control is essential for both microgrids [3] and transmission grids [4]. Transient stability emergency control (TSEC) is designed to keep the rotor angle synchronism after a severe fault. Generally, the special protection schemes (SPS) of the TSEC are summarized in two categories: closed-loop (response-driven) [5] and open-loop (event-driven) [6]. A flexible control strategy based on model predictive control (MPC) is proposed to ensure transient stability of the sending-end system [7], [8]. However, the wide-area measurement system-based closed-loop method [9], which is difficult to implement in practical projects, is hindered by communication signal delay. Transient stability emergency control is usually designed as an open-loop scheme to eliminate possible rotor instability by applying control measures that are stored in look-up tables beforehand, such as generator tripping and load shedding after severe disturbance [10].

With the large-scale integration of wind power, the mechanical inertia of the power system continues to decrease. Researchers have proposed tripping the wind turbine to improve transient stability [11], [12]. However, the dynamics of wind turbines are ignored. Meanwhile, even though the state-of-the-art forecasting method is adopted, wind power forecast error is about 10% in ultra-short-term wind prediction [13]. One of the significant challenges in TSEC research is obtaining robust emergency control strategies for grids with high wind power penetration.

Previous studies usually model the TSEC problem as a large-scale optimal control problem (OCP) with differential-algebraic equations (DAEs), which are typically deterministic and work only for a traditional system without uncertainty. When wind output power fluctuates over the predicted value, the robustness of the control strategy calculated in advance decreases.

To address the renewable energy uncertainty, the dynamic optimization framework, wherein the wind power is modeled as uncertainty sets, has been used with stochastic programming (SP) [14], robust optimization (RO) [15], and interval optimization (IO) [16] as summarized in Table 1. The SP is applied to solve transient stability constrained optimal power flow (TSCOPF), where a series of representative wind scenarios are constructed [14]. However, SP generally requires massive test scenarios to guarantee robustness. Compared with SP, RO and IO are the more conservative methods. The RO is a practical approach because the variation interval of the uncertainties is only required. The RO is applied to solve the preventive-corrective transient stability dispatch of power systems against wind power uncertainty and shows good performance on robustness [17]. However, the iterative method is time-consuming and may not be computationally reliable in practical application. IO is an appealing iteration-free method, which significantly improves computational efficiency [16]. Since the transient stability constraints are implicit and nonlinear, their bounds are difficult to obtain [18]. Meanwhile, high dimensional uncertainty greatly reduces computational efficiency. The linear approximation method is proposed to convert uncertain NLP to a deterministic optimization problem which improves optimization efficiency [16], [18]. Trajectory sensitivity, a by-product of time domain simulation (TDS), can quantitatively describe the linear relationship between uncertain parameters and transient stability constraints [19]. Once the bounds of transient stability constraints are established, the scale of TSEC is decreased and independent of the dimension of uncertainty.

As the scale of modern power system increases, another difficulty comes from DAEs constraints with complex dynamic component models. Up to now, different methods have been proposed to describe and simplify the DAEs constraints, also known as the direct method, such as transient energy function [20], extended equal area criterion (EEAC) [21], the stability region-based controlling unstable equilibrium point method (BCU) [22], single-machine equivalent [23] and the potential energy boundary surface (PEBS) method [24] as summarized in Table 1. A preventive generation rescheduling and corrective load-shedding method based on EEAC is proposed under wind power uncertainty [15]. However, simplification comes at the cost of violating reliability. With the development of artificial intelligence, an adaptive method based on deep reinforcement learning (DRL) is proposed to solve the TSEC problem [25]. However, the DRL-based TSEC has poor explainability and questionable accuracy, which can be used as a safety aid rather than a basis for emergency control.

With the rapid growth of modern computer computing capability, the indirect method based on accurate time simulation is adopted to solve the constraints. Numerical discretization, used to discretize the emergency control problem into a large-scale NLP, causes "curse of dimension". Previous research carries out a new parallel reduced-space interior point method to relieve the "curse of dimension" [26]. Furthermore, the direct sequential approach, in which the DAEs constraints are moved out of the OCP, is applied to improve calculation efficiency [27]. As a result, the simulation progress and small-scale NLP progress are solved separately. An improved mixed-integer TSEC approach, which formulates generator tripping and load shedding as discrete and continuous control variables, respectively [28]. To further improve the computational performance, a parallel block and control variable selection algorithm is proposed for large-scale power systems [29]. However, the above methods [26], [27], [28], [29] ignore the impact of wind power uncertainty on the control strategy as summarized in Table 1.

As a continuation of our previous works [27], [29], [30], we further extend the previous methods to the TSEC for high-penetration wind generation grids and formulate the robust transient stability emergency control (RTSEC) as a robust nonlinear programming (RNLP) problem. To ensure the transient stability of the system against wind power uncertainty, this paper provides an approach to generating control strategies. Compared to the previous works, there are several contributions from the proposed approach of this paper:

1) Robust transient stability emergency control is proposed where the uncertain wind power outputs are modeled as intervals. The worst case of wind power variation can be identified and addressed. Meanwhile, the wind turbine tripping model is also proposed to enhance system stability.

2) The approximation of transient stability constraint boundary based on trajectory sensitivity analysis can significantly improve the computational efficiency under the premise of ensuring accuracy.

The rest of this paper is organized as follows: the RTSEC formulation is discussed in Section II. Section III proposes the linear approximation method to obtain transient stability constraint for the worst case. Section IV shows the effectiveness of the proposed approach on two test systems. We summarize our conclusions in Section V.

II. FORMULATION OF RTSEC PROBLEM

Since the inertia of the power system decreases with the high penetration of power electronic devices, the transient process develops extremely rapidly in severe faults. The closed-loop-based control is too slow to eliminate transient instability after a serve disturbance [31]. As a result, the open loop control based on the SPS system, shown in Figure 1, is adopted [10]. The control strategies are predetermined considering possible operating scenarios and are saved in the control strategy tables. The automatic systems detect the fault location and the oncoming instability. The control strategies are implemented automatically by relay protection after the actual occurrence of a severe contingency.

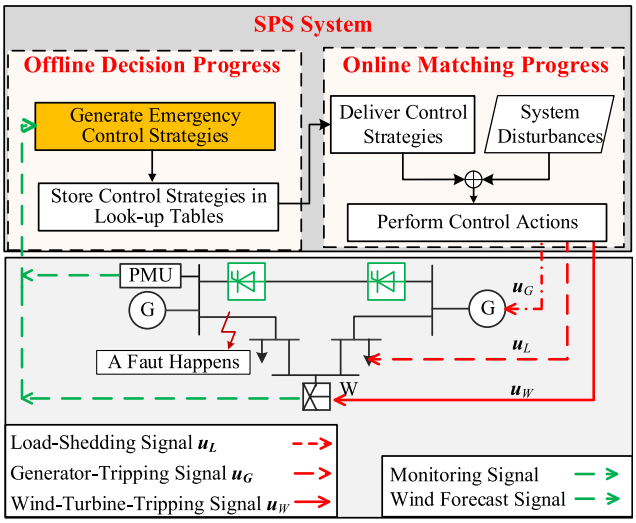

FIGURE 1. A sketch of TSEC framework.

Since the control strategy table is updated periodically less than 5 minutes [32], this open-loop scheme still requires high calculation efficiency and robustness, although the pre-calculation progress is offline.

A. RTSEC MODEL

To ensure the transient stability of grids against uncertain wind power generations, an optimization model is established to determine the control strategies as (1), subject to the constraint of rotor angle stability.

$$\min_{\boldsymbol{u}_G,\boldsymbol{u}_L,\boldsymbol{u}_W} \quad \boldsymbol{\Phi}(\boldsymbol{u}_L,\boldsymbol{u}_G,\boldsymbol{u}_W) \tag{1a}$$

$$s.t. \begin{cases} \dot{\boldsymbol{x}}(t) = \boldsymbol{f}(\boldsymbol{x}(t),\boldsymbol{y}(t),\boldsymbol{x}_0,\boldsymbol{y}_0,\boldsymbol{u},\boldsymbol{P}_u) & (1b) \\ \boldsymbol{0} = \boldsymbol{g}(\boldsymbol{x}(t),\boldsymbol{y}(t),\boldsymbol{x}_0,\boldsymbol{y}_0,\boldsymbol{u},\boldsymbol{P}_u) & (1c) \\ \boldsymbol{p}_0(\boldsymbol{P}_u) = \boldsymbol{0} & (1d) \\ \boldsymbol{I}(\boldsymbol{x}_0,\boldsymbol{y}_0,\boldsymbol{P}_u) = \boldsymbol{0} & (1e) \\ \underline{\boldsymbol{G}} \le \boldsymbol{G}(\boldsymbol{x}(t),\boldsymbol{y}(t),\boldsymbol{u},\boldsymbol{P}_u) \le \overline{\boldsymbol{G}} & (1f) \end{cases}$$

where the model (1) is a nonlinear programming model for transient stability emergency control. The dynamic equation (1b) includes wind turbines (WT) and synchronous generators (SG). Equation (1c) denotes the network equation. Equations (1b) and (1c) are the DAEs model of the power system. AC power flow constraint (1d), together with the initial condition equation (1e) are used to describe steady-state power flow and the state variables' initial value when the wind power varies. Constraint (1f) is the transient rotor angle constraint and control variable constraint. $\boldsymbol{x}$ and $\boldsymbol{y}$ are state variable vectors and algebraic variable vectors, respectively. The subscript 0 indicates the initial value of $\boldsymbol{x}$ and $\boldsymbol{y}$. $\boldsymbol{I}$ are initial condition equations. By solving such a large-scale RNLP, the control strategies $\boldsymbol{u}$, which include synchronous generator-tripping $\boldsymbol{u}_G$, wind-generation-tripping $\boldsymbol{u}_W$ and load-shedding

TABLE 1. Taxonomy of power system transient stability emergency control methods.

TSEC methods	Handling of DAE constraints	Uncertainty consideration	Iteration-free approach
Ref. [15]	Direct method	Yes (RO)	No
Ref. [17]	Direct method	Yes (SP)	Yes
Ref. [20]- [24]	Direct method	No	\
Ref. [26]	Indirect method (Numerical discretization)	No	\
Ref. [27]- [29]	Indirect method (sequential approach)	No	\
This work	Indirect method (sequential approach)	Yes	Yes

$\boldsymbol{u}_L$, can be generated. $\boldsymbol{P}_W$ is the mechanical power extracted from the wind, which will be defined in Section III. $t \in [0, T]$, T is the transient period.

B. OBJECTIVE FUNCTION

The objective function could be formulated as the following form, which is the minimum cost of the active power of tripping generators and shedding loads:

$$\boldsymbol{\Phi}(\boldsymbol{u}) = \sum_{i=1}^{n_L} c_{Li} u_{Li} P_{Li} + \sum_{i=1}^{n_G} c_{Gi} u_{Gi} P_{Gi} + \sum_{i=1}^{n_W} c_{Wi} u_{Wi} P_{Wi} \tag{2}$$

where n_G, n_W and n_L are the numbers of tripping SG, tripping WT and shedding load. P_{Gi}, P_{Wi} and P_{Li} denote the power of the SG-tripping buses, WT-tripping buses and load-shedding buses, respectively.

C. DYNAMIC CONSTRAINTS

The TSEC model for synchronous generators and the LCC-HVDC model are easily found in [29] and [30]. Permanent magnet synchronous generators (PMSG) have been widely used due to their high flexibility and lightweight. The tripping model of wind turbines is proposed based on PMSG in this paper. The tripping model of doubly-fed induction generators can be derived from the same method.

The various dynamic models of PMSG for transient stability analysis have been proposed in [33] and [34]. Under the assumption: (1) Electromagnetic transients are neglected; (2) Voltage and current are fundamental frequency sinusoidal waves, the PMSG model is described below:

1) Turbine mechanical model

$$\frac{d\omega_m}{dt} = \frac{1}{2H_m}\left(\frac{P_W}{\omega_m} - T_e\right) \tag{3}$$

The mechanical power P_W extracted from the wind is modeled as uncertain intervals, shown in Section III.

The electrical power T_e is:

$$T_e = \left(\psi_s + \left(x_{qs} - x_{ds}\right) i_{ds}\right) i_{qs} \tag{4}$$

2) Converter and control model for PMSG

The converter is modeled as an ideal current source after the converter dynamic is simplified [30]. On the grid-side converter, the voltage control is adopted to keep the voltage on the interconnect point a given reference voltage v_{ref} which is expressed as follows:

$$\frac{di_{dc}}{dt} = \frac{1}{T_v}(k_v(v_{ref} - v) - i_{dc}) \tag{5}$$

where v is the grid voltage.

On the generator-side converter, the active power is controlled by varying the q-axis current:

$$\frac{di_{qs}}{dt} = \frac{1}{T_{ep}}\left(\frac{P_W^*}{\omega_m \psi_s - x_{ds} i_{ds}} - i_{qs}\right) \tag{6}$$

where the optimal mechanical power P_W^* is determined from an experimental curve relating wind energy capture to mechanical speed for each value of the rotor speed ω_m [33], [34]. It is assumed that $P_W^* = 0$ if $\omega_m \leq 0.5\,p.u.$, that $P_W^* = 1\,p.u.$ if $\omega_m > 1.0\,p.u.$ that $P_W^* = 2\omega_m - 1$ if $0.5\,p.u. < \omega_m < 1.0\,p.u.$ as shown in Figure 2.

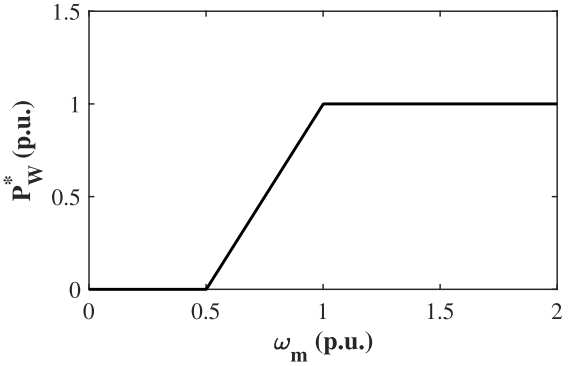

FIGURE 2. Wind turbine power control reference curve.

Assuming that active power on the DC line is lossless and the generator-side converter power factor is equal to 1, thus the following equations hold:

$$0 = P_s - P_c \tag{7a}$$

$$0 = Q_s \tag{7b}$$

3) Wind generation tripping model

Assume that the wind generators on the same node i have the same parameters. After the wind generators with the ratio

of u_{Wi} are tripped, the corresponding dynamic parameters of wind generation change as follows:

$$\begin{aligned} x_{ds}^1 &= (1-u_{Wi})\, x_{ds} \\ x_{qs}^1 &= (1-u_{Wi})\, x_{qs} \\ \psi_s^1 &= (1-u_{Wi})\, \psi_s \\ H_m^1 &= (1-u_{Wi})\, H_m \\ P_c^1 &= (1-u_{Wi})\, P_c \end{aligned} \tag{8}$$

where superscript 1 denotes the dynamic parameters after the wind generators are tripped. After equation (8) is substituted in equation (3)-(6), It can be found that the differential equation of the equivalent wind generators is exactly the same before and after tripping the wind turbines.

4) Network model

The network equations $\boldsymbol{g}$ are shown below:

$$\begin{bmatrix} \boldsymbol{G} & -\boldsymbol{B} \\ \boldsymbol{B} & \boldsymbol{G} \end{bmatrix} \begin{bmatrix} \boldsymbol{V}_x \\ \boldsymbol{V}_y \end{bmatrix} = \begin{bmatrix} \boldsymbol{I}_x \\ \boldsymbol{I}_y \end{bmatrix} \tag{9}$$

where $\boldsymbol{V}_x$ and $\boldsymbol{V}_y$ represent the real and imaginary parts of bus voltages, $\boldsymbol{I}_x$ and $\boldsymbol{I}_y$ represent the real and imaginary parts of injected currents, $\boldsymbol{G}$ and $\boldsymbol{B}$ represent the real and imaginary parts of the bus admittance matrix, respectively.

The injected current I_{xw}, I_{yw} for wind turbine tripping nodes i is expressed as:

$$I_{xw} = (1-u_{Wi})\,\frac{P_c V_{xw} + Q_c V_{yw}}{V_{xw}^2 + V_{yw}^2}, \tag{10a}$$

$$I_{yw} = (1-u_{Wi})\,\frac{P_c V_{yw} - Q_c V_{xw}}{V_{xw}^2 + V_{yw}^2} \tag{10b}$$

Based on (10a) (10b), the injected current of generator-tripping buses and load-shedding nodes $I_{xi}(t)$, $I_{yi}(t)$ could be rewritten as:

$$\begin{aligned} I_{xi}(t) &= (1-u_{ki}) C_i^x (V_{xi}, V_{yi}, x_{ki}) \\ I_{yi}(t) &= (1-u_{ki}) C_i^y (V_{xi}, V_{yi}, x_{ki}) \end{aligned} \tag{11}$$

where i denotes the i-th bus. C_i^x and C_i^y represent different kinds of dynamic components. u_k stands for the proportion of generator tripping or load shedding.

D. TRANSIENT STABILITY CONSTRAINTS

The absolute deviation of rotor angle with respect to the center of inertia (COI), which has to be within a certain degree $\overline{\delta}$, is utilized as the criterion of transient rotor angle stability:

$$-\overline{\delta} \le \delta_i(t) - \delta_{COI}(t) \le \overline{\delta} \quad t \in [0, T] \tag{12}$$

where δ_{COI} denotes:

$$\delta_{COI} = \frac{\sum_{i=1}^{N_G} T_{Ji}\delta_i(t)}{\sum_{i=1}^{N_G} T_{Ji}} \tag{13}$$

Since handling path constraints is challenging, the constraint transformation method [27], [35] is employed to reformulate rotor angle constraints. For each $i = 1, \ldots, N_G$, the corresponding continuous state inequality constraint in (12) is equivalent to

$$\theta\left(x\left(t|\boldsymbol{u}\right)\right) = \max_i \left\{(\delta_i(t|\boldsymbol{u}) - \delta_{COI}(t|\boldsymbol{u}))^2, i = 1, \ldots, N_G\right\} - \overline{\delta}^2 \leqslant 0 \quad t \in [0, T] \tag{14}$$

where $(t|\boldsymbol{u})$ represents the variable values when control variables are $\boldsymbol{u}$ at the moment t.

We define $\tilde{\theta}\left(x\left(t|\boldsymbol{u}\right)\right)$ as follows:

$$\tilde{\theta}\left(x\left(t|\boldsymbol{u}\right)\right) = \max\left\{0, \theta\left(x\left(t|\boldsymbol{u}\right)\right)\right\} \quad t \in [0, T] \tag{15}$$

If the transient stability constraint is satisfied during the period $t \in [0, T]$, $\theta\left(x\left(t|\boldsymbol{u}\right)\right)$ is always zero. Finally, the path constraints can be replaced as integral constraints form:

$$h\left(u\right) = \int_0^T \tilde{\boldsymbol{\theta}}\left(x\left(t|\boldsymbol{u}\right)\right) dt = 0 \tag{16}$$

The path constraint (12) is now converted to integral constraint (16). In order to increase the numerical stability of the algorithm, a very small positive constant ε is added to slack the constraint:

$$h(\boldsymbol{u}) \le \varepsilon \tag{17}$$

where ε is a positively small number, about 10^{-3}.

The upper boundary and lower boundary constraints of $\boldsymbol{u}_{Gi}$, $\boldsymbol{u}_{Li}$ and $\boldsymbol{u}_{Wi}$ are:

$$\begin{cases} 0 \le \boldsymbol{u}_{Gi} \le 1 & i = 1, \ldots, r_G \\ 0 \le \boldsymbol{u}_{Li} \le 1 & i = 1, \ldots, r_L \\ 0 \le \boldsymbol{u}_{Wi} \le 1 & i = 1, \ldots, r_W \end{cases} \tag{18}$$

where we suppose that the proportion of generator tripping u_{Gi} and u_{Wi} are continuous variables. The same assumption is also adopted in [27] and [29].

III. TRANSIENT STABILITY CONSTRAINT FOR WORST CASE

A. WIND POWER UNCERTAINTY MODELLING

In the RTSEC model (1), the mechanical power $\boldsymbol{P}_W$ extracted from the wind is modeled as an uncertainty interval given below:

$$\boldsymbol{P}_{Wi} \in \left[P_{Wi}^{min}, P_{Wi}^{max}\right] \quad i = 1, \ldots, N_W \tag{19}$$

In this uncertainty interval, the i-th uncertainty variable $\boldsymbol{P}_{Wi}$ is limited between the lower bound P_{Wi}^{min} and upper bound P_{Wi}^{max}. The P_{Wi}^{min} and P_{Wi}^{max} can be obtained by wind prediction techniques [36].

Compared to the predicted wind power, the actual wind power outputs are limited within the lower and upper bound. In order to identify the power angle instability caused by wind power output in the worst conditions, any possible wind power output is treated equally, even in extreme cases with a small probability of occurrence. Based on this assumption, extreme wind output is as likely to occur as any value within

the specified range. Therefore, the system's stability is guaranteed against any possible wind power output within the uncertainty interval.

B. TRANSIENT STABILITY CONSTRAINT APPROXIMATION

Since the transient stability constraints $h(\boldsymbol{u}, \boldsymbol{P}_{Wi})$ are implicit and nonlinear, their bounds are difficult to obtain when the interval optimization is applied to solve the NLP.

According to the requirements of special protection systems, transient stability emergency control strategy tables are updated periodically in less than 5 minutes [32]. During this period, the error of ultra-short-term wind power forecasting is less than 5% in China [26]. The first-order trajectory sensitivity approximation ensures an approximation accuracy in this case of wind power error, which will be verified in Section IV. The first-order trajectory sensitivity approximation can overcome the need for repetitive simulation.

The worst-case transient rotor angle stability constraint based on first-order approximation is expressed as:

$$h(\boldsymbol{u}, \boldsymbol{P}_{Wi}) \approx h_0(\boldsymbol{u}, \boldsymbol{P}_{Wi0}) + \boldsymbol{M}^{(1)} \Delta \boldsymbol{P}_{Wi} \tag{20}$$

where $\boldsymbol{h}_0(\boldsymbol{u}, \boldsymbol{P}_{Wi0})$ is the nominal trajectory constraint as wind power outputs are $\boldsymbol{P}_{Wi0}$. $\boldsymbol{M}^{(1)}$ is defined as a first-order disturbance factor, which is utilized to describe the influence of uncertain variables $\boldsymbol{P}_{Wi}$ on transient rotor angle stability. $\Delta \boldsymbol{P}_{Wi}$ is the power deviation between the worst and nominal cases.

$$\begin{aligned} \boldsymbol{M}^{(1)} &= \left. \frac{\partial h(\boldsymbol{u}, \boldsymbol{P}_{Wi})}{\partial \boldsymbol{P}_{Wi}} \right|_{\boldsymbol{P}_{Wi}=\boldsymbol{P}_{Wi0}} = \int_{t=0}^{T} \frac{\partial \tilde{\theta}}{\partial \boldsymbol{P}_{Wi}} dt \\ &= \int_{t=0}^{T} \frac{\partial \tilde{\theta}}{\partial \boldsymbol{x}} \frac{\partial \boldsymbol{x}}{\partial \boldsymbol{x}_0} dt \frac{\partial \boldsymbol{x}_0}{\partial \boldsymbol{P}_{Wi}} \end{aligned} \tag{21}$$

where the trajectory sensitivity $\partial \boldsymbol{x} / \partial \boldsymbol{x}_0$ is obtained through the method proposed in [19]. $\partial \boldsymbol{x}_0 / \partial \boldsymbol{P}_{Wi}$ denotes the influence of power disturbance on the initial value $\boldsymbol{x}_0$, which can be obtained from power flow equations $\boldsymbol{p}_0$ and initial condition equations $\boldsymbol{I}$.

As the affine transformation (4) maintains convexity [19], the boundary of transient stability constraint can be immediately determined through (21)(22). However, n uncertainties will cause $2n$ boundary trajectories which are computationally intractable. Considering that not all boundary trajectories are necessary, the worst case of $h(\boldsymbol{u}, \boldsymbol{P}_{Wi})$ is obtained by setting the i-th element of $\Delta \boldsymbol{P}_{Wi}$ according to

$$\Delta \boldsymbol{P}_{Wi} = \begin{cases} \dfrac{P_{Wi}^{\max} - P_{Wi}^{\min}}{2}, & \text{if } \boldsymbol{M}_i^{(1)} > 0 \\ \dfrac{P_{Wi}^{\min} - P_{Wi}^{\max}}{2}, & \text{if } \boldsymbol{M}_i^{(1)} < 0 \end{cases} \tag{22}$$

According to the sign of $\boldsymbol{M}_i^{(1)}$, the worst case of wind power can be identified and addressed within the uncertainty interval.

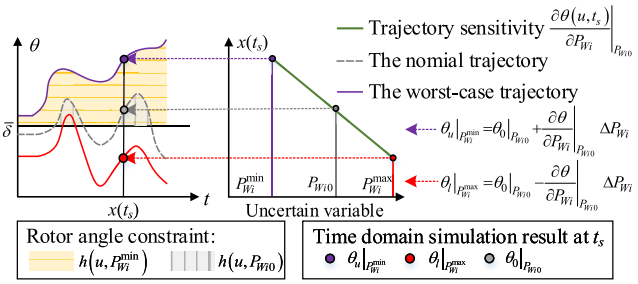

FIGURE 3. Illustrate of constraint approximate under uncertainties.

The above transient stability constraint approximate method based on trajectory sensitivity analysis is illustrated in Figure 3. Figure 3 shows that the points on the perturbed trajectory θ_u (or θ_l) can be computed by the point θ_0 and trajectory sensitivity $\partial \theta / \partial \boldsymbol{P}_{Wi}$. The trajectory sensitivity analysis will be illustrated as follows.

C. TRAJECTORY SENSITIVITY ANALYSIS

For power system dynamics, the first-order trajectory sensitivities can be analytically calculated as a byproduct of times domain simulation (TDS) with implicit integration techniques such as the trapezoidal method.

At time step t, after applying the chain rule of differentiation to DAEs (1b)-(1c), the sensitivities of state variables with respect to control variables $\boldsymbol{u}$ (or wind power output $\boldsymbol{P}_{Wi}$) are obtained:

$$\begin{aligned} &\begin{bmatrix} \dfrac{\partial \boldsymbol{f}}{\partial \boldsymbol{x}_t} & \dfrac{\partial \boldsymbol{f}}{\partial \boldsymbol{V}_t} \\ \dfrac{\partial \boldsymbol{g}}{\partial \boldsymbol{x}_t} & \dfrac{\partial \boldsymbol{g}}{\partial \boldsymbol{V}_t} \end{bmatrix} \begin{bmatrix} \dfrac{d\boldsymbol{x}_t}{d\boldsymbol{u}} \\ \dfrac{d\boldsymbol{V}_t}{d\boldsymbol{u}} \end{bmatrix} \\ &= - \begin{bmatrix} \dfrac{\partial \boldsymbol{f}}{\partial \boldsymbol{x}_{t-1}} \dfrac{d\boldsymbol{x}_{t-1}}{d\boldsymbol{u}} + \dfrac{\partial \boldsymbol{f}}{\partial \boldsymbol{V}_{t-1}} \dfrac{d\boldsymbol{V}_{t-1}}{d\boldsymbol{u}} + \dfrac{\partial \boldsymbol{f}}{\partial \boldsymbol{u}} \\ \dfrac{\partial \boldsymbol{g}}{\partial \boldsymbol{u}} \end{bmatrix} \end{aligned} \tag{23}$$

Note that the coefficient matrix of the linear equation in (23) is the same as the Jacobian matrix in TDS. So after solving the discretized DAE system at time step t, the computed LU-decomposition of the Jacobian matrix in the last Newton step can be reused. In this way, the sensitivities can be calculated in parallel with the TDS. The detailed TDS and trajectory sensitivity analysis can be found in [19].

D. PROCEDURE FLOW

The direct sequential approach, also known as direct single shooting or control vector parameterization, transcribes the dynamic optimization problem and then solves the yielded parametric nonlinear optimization problem (NLP) [37]. To improve the efficiency, the primal-dual interior point method (IPM) [38] is an efficient algorithm to solve the complex NLP. When the predictor-corrector IPM is utilized to solve the NLP (1), the second-order trajectory sensitivity, also known as the Hessian matrix, is desired. Since it is

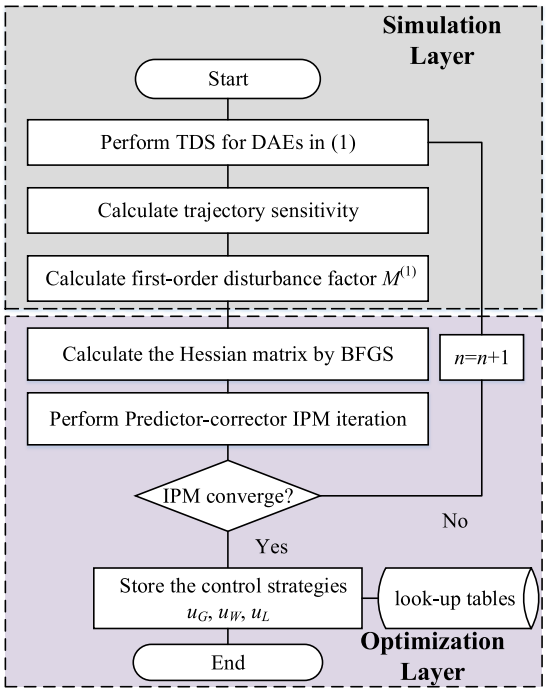

FIGURE 4. Flowchart of the proposed approach.

difficult to obtain the precise Hessian matrix of the constraints directly, the approximate Hessian matrix is obtained by the Broyden-Fletcher-Goldfarb-Shanno (BFGS) method, which is introduced in detail in [39] and will not be repeated here. In the proposed approach, there are two layers including the simulation layer and the optimization layer which are shown in Figure 4.

The overall process of RTSEC can be summarized as follows:

Step 1) **Initialization:** Set the control variables vector $\boldsymbol{u} = 0$, parameters of the predictor-corrector IPM and the initial Hessian matrix; set the iteration number $n = 0$.

Step 2) **Forward simulation:** Solve the power system DAE (1b) - (1c) by the implicit trapezoidal method.

Step 3) **Trajectory sensitivity analysis:** The gradients of constraints are obtained from equation (23). Calculate the Hessian matrix by BFGS method.

Step 4) **First-order disturbance factor:** Calculate first-order disturbance factor $\boldsymbol{M}^{(1)}$ by (21).

Step 5) **Solve the NLP:** The TSEC model (1) is solved by the predictor-corrector IPM [38].

Step 6) **Convergence criterion:** Examine whether the convergence state is achieved. If yes, the iterative process stops; otherwise, reset $n = n + 1$ and proceed to Step 2.

IV. CASE STUDY

A. SIMULATION SETTING

The proposed method is tested on a modified China Electric Power Research Institute (CEPRI) 22-bus system and a modified IEEE 300-bus system. The CEPRI 22-bus system includes 5 generators, 1 wind farm, and 1 HVDC, as shown in Figure 5. MATLAB is used to implement the proposed approach. The wind farm W1 power interval is set as [427.5 MW, 472.5 MW].

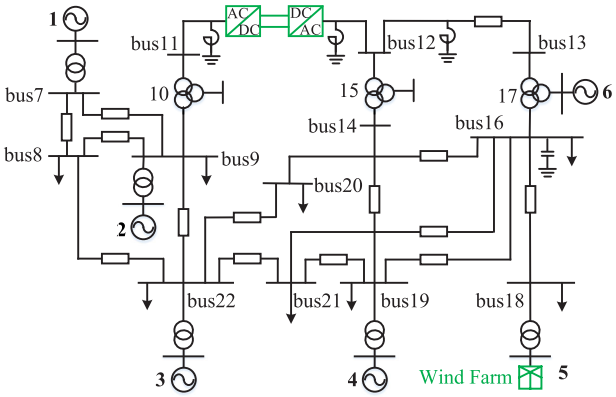

FIGURE 5. CEPRI 22-bus system with wind farm.

To further investigate the proposed method, a modified IEEE 300-bus system is tested, which consists of 300 buses, 69 generators, 410 transmission lines, and 199 loads. PMSGs of the same capacity replace the synchronous generators at buses 68, 69, 122.

The simulation time window is set to 3.5s, while the simulation time step for implicit trapezoidal integration is 0.02s. The contingency in this paper is initiated by three-phase to ground fault(s), which is cleared by tripping the fault line. The emergency control measurements are set to be taken at 0.2s after the fault lines clearance. Six fault scenarios are tested (see Table 2). Scenarios S1, S2, S4, S5 and S6 are tested in CEPRI 22-bus system. Scenario S3 is tested in IEEE 300-bus system.

B. VERIFICATION OF TRANSIENT TRAJECTORY APPROXIMATE

Considering the nonlinear power system model, the error comes from ignoring higher-order terms. Generally, the high-order terms cannot be computed accurately unless extensive simulations. To test trajectory approximation accuracy, a deviation evaluation index is defined:

$$Error = \frac{\delta^A(t) - \delta^N(t)}{\delta^N(t)} \times 100\% \tag{24}$$

where the nominal trajectories $\delta^N(t)$ are obtained at the predicted wind power output without emergency control. The approximate upper (or lower) bound trajectories $\delta^A(t)$ are calculated by trajectory sensitivities approximation.

From Figure 6 and Figure 7, one can find that the most deviation is less than 2.1% under Scenario S1 and 0.12% under Scenario S3. The approximate worst-case trajectories for rotor angles closely track the actual worst-case trajectories. It can be found that the impacts of wind forecast errors can be evaluated during a single simulation progress.

TABLE 2. Fault scenario sets.

Scenario sets	Fault bus	Fault duration time (s)	Tripped line	fault type
Scenario S1	16	0.30	16-20	Three-phase fault
Scenario S2	19	0.30	19-21	Three-phase fault
Scenario S3	3	0.20	3-129	Three-phase fault
Scenario S4	19	0.30	19-21	Single line-to-ground fault
Scenario S5	19	0.30	19-21	Line-to-line fault
Scenario S6	19	0.30	19-21	Double line-to-ground fault

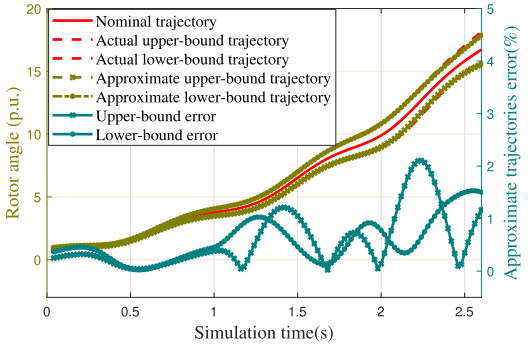

FIGURE 6. Error comparison of approximate trajectory and actual trajectory. (CEPRI 22-bus system.)

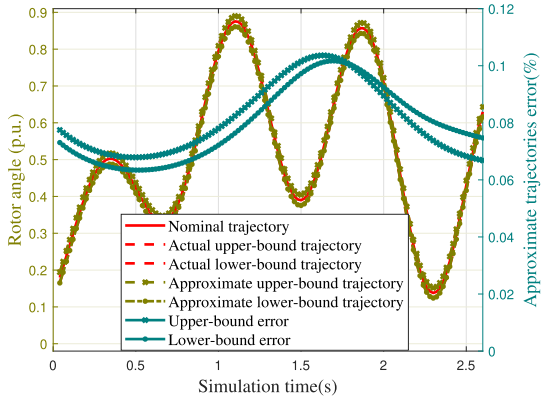

FIGURE 7. Error comparison of approximate trajectory and actual trajectory. (IEEE 300-bus system.)

TABLE 3. Error comparison for transient stability constraint.

Worst-case transient stability constraint $h(\boldsymbol{u})$	Scenario S1	Scenario S2	Scenario S3
Nominal	58.636	49.364	19.321
Approximate	57.834	47.729	19.329
Error (%)	1.367%	3.312%	0.041%

For further verification, Table 3 provides the nominal and approximate worst-case transient stability constraints $h(\boldsymbol{u})$ at $\boldsymbol{u} = \mathbf{0}$. The approximation errors of the above three scenarios S1, S2, and S3 are less than 3.5% compared with the actual

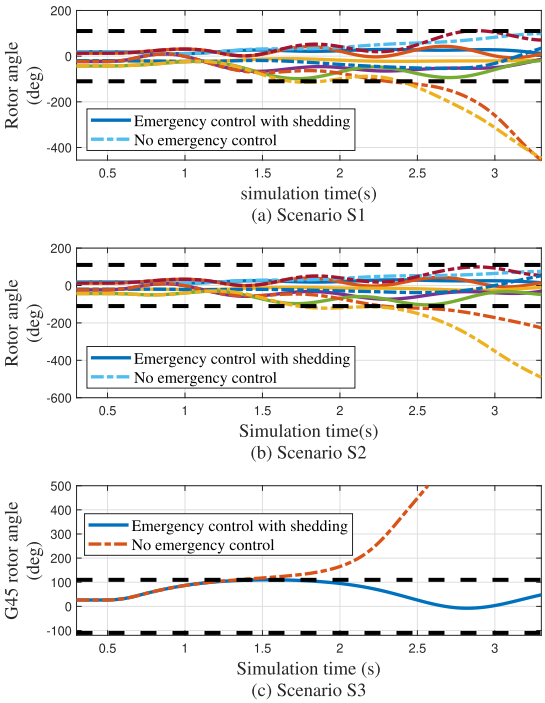

FIGURE 8. Time simulation verification under the nominal case.

computed worst-case transient stability constraints. The trajectory sensitivity analysis provides credible worst-case transient stability constraint information for optimization. Since the trajectory sensitivity analysis is accompanied by simulation progress, the proposed method avoid repeated simulation calculations and improves computation efficiency.

C. TIME SIMULATION VERIFICATION

To illustrate the effectiveness of emergency control, time-domain simulations are carried out after the control actions are taken on three fault scenarios.

Table 4 shows the optimization results by the proposed method, including the number of shedding loads n_L, the number of tripped synchronous generators n_G, the number of tripped wind generators n_W, the loads shedding total power P_{TL}, generators tripped total power P_{TG} and the wind generators tripped total power P_{TW}. As shown in Table 4, tripping the wind generator, together with tripping generators

TABLE 4. TSEC strategies under different scenarios.

Control strategy	Scenario S1	Scenario S2	Scenario S3	Scenario S4	Scenario S5	Scenario S6
n_L	0	0	1	1	0	0
n_G	1	2	2	2	2	0
n_W	0	0	1	1	0	0
P_{TL} (MW)	0	0	15.29	20.58	0	0
P_{TG} (MW)	165.67	180.57	728.17	373.88	107.72	0
P_{TW} (MW)	0	0	26.97	193.58	0	0

and shedding loads, engages in the improvement of system stability under Scenario S1 and Scenario S3.

Figure 8 gives the simulation results obtained under three test cases. Rotor angle curves are shown in Figure 8. The dotted lines demonstrate that the generator rotors are out of synchronization without any control measures. As the solid lines show, all rotor angles are within the limitations after the TSEC takes action.

Figure 9 shows the trajectory of generator G5 rotor angle is within the limitations after applying the TSEC strategies when wind power varies in [427.5 MW, 472.5 MW]. The black curve is the approximate boundary obtained by trajectory sensitivity analysis. The perturbed trajectories (red lines) lie in the pink region bounded by the black dotted line. From Figure 8 and Figure 9, we can find that the TSEC strategies effectively avoid transient instabilities under uncertain wind power generations. In both Scenario S1 and Scenario S2, the worst-case transient stability constraints are reached when the actual wind power is 427.5 MW.

The worst case of wind power is shown in the red dots in Figure 10. The mean wind power outputs of three distinct wind farms and their forecasted intervals are represented by hollow circles and blue lines, respectively. The wind power intervals of wind farms W1, W2 and W3 power in [348.27MW, 384.93MW], [256.22MW, 283.18 MW,] and [130.73MW, 144.48 MW], respectively. It can be found that the worst-case transient stability constraint reaches when the wind farms W1, W2 and W3 operate at 384.93 MW, 283.18 MW and 144.48 MW, respectively. In the current fault scenario, the greater the wind speed and power output, the easier the system loses stability.

When referring to the unbalanced faults, the only correction of the proposed method is the effective fault impedance. The negative-sequence impedance and zero-sequence impedance of synchronous generators can be calculated following [40]. The negative sequence impedance of PMSG can be calculated following [41].

As shown in Table 4, tripping the wind generator, together with tripping generators and shedding loads, engage in the improvement of system stability under Scenario S4, S5. Since the rotor angles keep stability under Scenario S6, no additional control strategies are needed.

Figure 11 gives the simulation results obtained under unbalanced faults when the wind power output is 450MW.

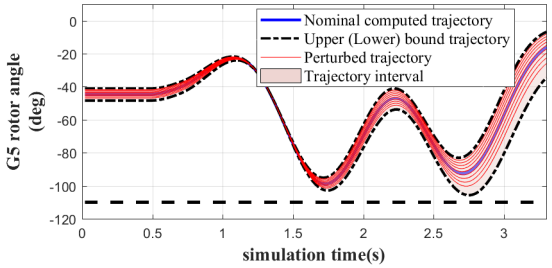

FIGURE 9. Trajectories of rotor angle G5 for varying wind power.

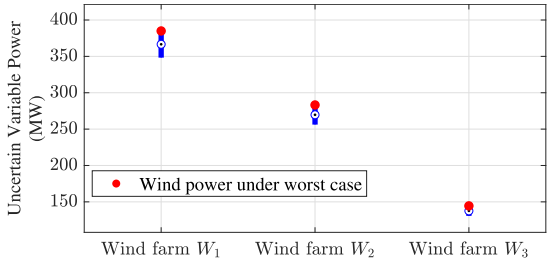

FIGURE 10. Explanation of the worst case for wind power.

Rotor angle curves are shown in Figure 11. The dotted lines demonstrate that the generator rotors are out of synchronization without any control measures under scenarios S4 and S5. As the solid lines show, all rotor angles are within the limitations after the TSEC takes action under scenarios S4 and S5. When the double line-to-grand fault happens at bus 19, the rotor angles keep stability without control measures.

D. ROBUSTNESS PERFORMANCE

To verify the effectiveness of the proposed method in this paper, the acceleration energy (AE)-based transient stability emergency control [4] is tested. Meanwhile, the deterministic optimization method [27] and the scenario-based method [17] are also tested.

Figure 12 is the time domain simulation result of the rotor angle of generator G5 when the wind power is 427.5MW under Scenario S2. As shown in Figure 12, we can find that the proposed method is still available when the wind power output reaches the worst case. However, the rotor angles will lose synchronization if the control strategies generated by the AE-based method and the deterministic method are applied to

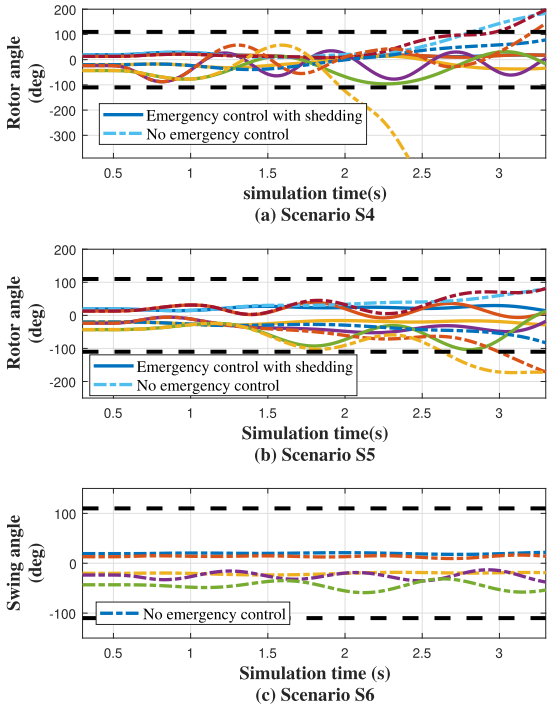

FIGURE 11. Time simulation verification under unbalanced faults.

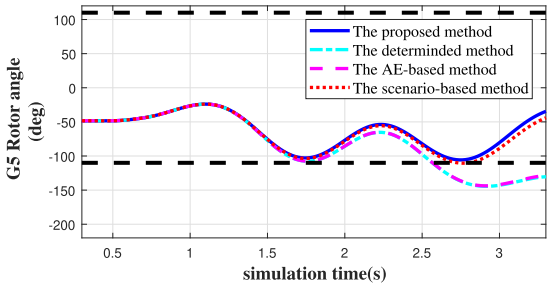

FIGURE 12. Rotor angle curve under worst-case wind power with TSEC.

the 22-bus system. When the wind power reaches the lower bound, the proposed method shows good performance on robustness.

A stability robustness evaluation for the two scenarios is carried out. The results are given in Table 5. To test the robustness of the control strategies, a stability robustness index [17] is defined as follows:

$$\eta = \frac{N_s}{N} \tag{25}$$

where N is the total number of random scenarios randomly produced within the interval. The N_s is the number of stable scenarios. This paper sets the total number of test cases as 100.

For comparison, a deterministic optimization method [27] is also tested, which generates the control strategies under the nominal case. Table 5 indicates that the proposed method improves the robustness of emergency control strategies compared with the deterministic method and the AE-based method. As shown in Table 5, the rotor angles are out-of-step

TABLE 5. Robust performance under different fault scenarios.

Fault scenarios	Stability robustness η	
	Scenario S1	Scenario S2
The deterministic method [27]	91%	89%
The AE-based method [4]	89%	89%
The scenario-based method [17]	100%	100%
The proposed method	100%	100%

TABLE 6. Computational performance of the proposed method.

Fault scenarios	CPU time (s)	
	Scenario S1	Scenario S2
The scenario-based method [17]	237.27	251.51
The proposed method	70.59	50.57

under about 10% of wind output scenarios if the deterministic or AE-based method is adopted. Table 5 indicates that the proposed method improves the robustness of emergency control strategies compared with the deterministic method. It can be observed that the proposed approach significantly outperforms compared with the scenario-based method [17] in CPU time in Table 6.

V. CONCLUSION

This work proposes a robust TSEC strategy generation approach to eliminate possible rotor angle instability considering wind power output uncertainty which mainly results from the wind power prediction. Simulations are performed on the 22-bus system and the modified 300-bus system, which show that the proposed approach can improve the system stability for different contingencies and have a good dynamic response. The conclusions are summarized:

1) The control strategies generated by the proposed method maintain the transient rotor angle stability robustly against wind power uncertainty in contrast to a deterministic method.

2) The worst-case transient stability constraints can be obtained with only one-time TDS with the help of trajectory sensitivity. Thus, the cost time of optimization can be significantly reduced over the conventional methods.

For future work, the energy storage systems can be integrated into the proposed TSEC model for the improvement of transient stability. In addition, as only the wind power uncertainty is considered in this work, the effect of photovoltaic uncertainty can be further investigated.

REFERENCES

[1] E. Vittal, M. O'Malley, and A. Keane, "Rotor angle stability with high penetrations of wind generation," *IEEE Trans. Power Syst.*, vol. 27, no. 1, pp. 353–362, Feb. 2012.

[2] National Grid ESO. (Aug. 2019). *Interim Report Into the Low-Frequency Demand Disconnection (LFDD)*. [Online]. Available: https://www.nationalgrideso.com/ducument/151081/download

[3] S. A. G. K. Abadi and A. Bidram, "Effective utilization of grid-forming cloud hybrid energy storage systems in islanded clustered DC nano-grids for improving transient voltage quality and battery lifetime," *IET Gener. Transmiss. Distrib.*, 2023, doi: 10.1049/gtd2.12775.

[4] H. Ota, Y. Kitayama, H. Ito, N. Fukushima, K. Omata, K. Morita, and Y. Kokai, "Development of transient stability control system (TSC system) based on on-line stability calculation," *IEEE Trans. Power Syst.*, vol. 11, no. 3, pp. 1463–1472, Aug. 1996.

[5] W. Wang, X. Xiong, M. Li, and R. Yu, "A flexible control strategy to prevent sending-end power system from transient instability under HVDC repetitive commutation failures," *IEEE Trans. Power Syst.*, vol. 35, no. 6, pp. 4445–4458, Nov. 2020.

[6] T. Xiao, Y. Zou, Y. Xia, W. Tong, Y. Gao, and J. Wang, "Design and tests of a super real-time simulation-based power system real-time decision-making emergency control system," *IET Gener., Transmiss. Distrib.*, vol. 14, no. 9, pp. 1714–1725, May 2020.

[7] S. Das and B. K. Panigrahi, "Prediction and control of transient stability using system integrity protection schemes," *IET Gener., Transmiss. Distrib.*, vol. 13, no. 8, pp. 1247–1254, Apr. 2019.

[8] S. A. G. K. Abadi, S. I. Habibi, T. Khalili, and A. Bidram, "A model predictive control strategy for performance improvement of hybrid energy storage systems in DC microgrids," *IEEE Access*, vol. 10, pp. 25400–25421, 2022.

[9] R. Yousefian, R. Bhattarai, and S. Kamalasadan, "Transient stability enhancement of power grid with integrated wide area control of wind farms and synchronous generators," *IEEE Trans. Power Syst.*, vol. 32, no. 6, pp. 4818–4831, Nov. 2017.

[10] Z. Yao, V. R. Vinnakota, Q. Zhu, C. Nichols, G. Dwernychuk, and T. Inga-Rojas, "Forewarned is forearmed: An automated system for remedial action schemes," *IEEE Power Energy Mag.*, vol. 12, no. 3, pp. 77–86, May 2014.

[11] J. Ding, Y. Qiu, H. Sun, H. Zhou, S. Ma, Z. Wang, H. Shen, B. Li, and Y. Song, "Consideration of wind generator tripping under large-scale wind power integration," *Proc. CSEE*, vol. 31, no. 19, pp. 25–36, 2011.

[12] Q. Chen, H. Wang, and T. Littler, "Tripping control for transient stability in coordinated hydro and wind generation," in *Proc. 2nd IET Renew. Power Gener. Conf. (RPG)*, 2013, pp. 1–4.

[13] Y. T. Zhou, C. Jiang, and X. Han, "Interval and subinterval analysis methods of the structural analysis and their error estimations," *Int. J. Comput. Methods*, vol. 3, no. 2, pp. 229–244, Jun. 2006.

[14] S. Xia, X. Luo, K. W. Chan, M. Zhou, and G. Li, "Probabilistic transient stability constrained optimal power flow for power systems with multiple correlated uncertain wind generations," *IEEE Trans. Sustain. Energy*, vol. 7, no. 3, pp. 1133–1144, Jul. 2016.

[15] H. Yuan, Y. Xu, and C. Zhang, "Robustly coordinated generation dispatch and load shedding for power systems against transient instability under uncertain wind power," *IEEE Trans. Power Syst.*, vol. 37, no. 2, pp. 1032–1043, Mar. 2022.

[16] C. Jiang, Z. G. Zhang, Q. F. Zhang, X. Han, H. C. Xie, and J. Liu, "A new nonlinear interval programming method for uncertain problems with dependent interval variables," *Eur. J. Oper. Res.*, vol. 238, no. 1, pp. 245–253, Oct. 2014.

[17] H. Yuan and Y. Xu, "Preventive-corrective coordinated transient stability dispatch of power systems with uncertain wind power," *IEEE Trans. Power Syst.*, vol. 35, no. 5, pp. 3616–3626, Sep. 2020.

[18] C. Zhang, H. Chen, Z. Liang, M. Guo, D. Hua, and H. Ngan, "Reactive power optimization under interval uncertainty by the linear approximation method and its modified method," *IEEE Trans. Smart Grid*, vol. 9, no. 5, pp. 4587–4600, Sep. 2018.

[19] I. A. Hiskens and J. Alseddiqui, "Sensitivity, approximation, and uncertainty in power system dynamic simulation," *IEEE Trans. Power Syst.*, vol. 21, no. 4, pp. 1808–1820, Nov. 2006.

[20] Z. Yao, "A control-oriented energy function for generation shedding determination for transient stability control," *IEEE Trans. Power Syst.*, vol. 34, no. 1, pp. 413–421, Jan. 2019.

[21] Y. Xue, T. Van Custem, and M. Ribbens-Pavella, "Extended equal area criterion justifications, generalizations, applications," *IEEE Trans. Power Syst.*, vol. 4, no. 1, pp. 44–52, Feb. 1989.

[22] H.-D. Chiang, F. F. Wu, and P. P. Varaiya, "A BCU method for direct analysis of power system transient stability," *IEEE Trans. Power Syst.*, vol. 9, no. 3, pp. 1194–1208, Aug. 1994.

[23] A. Pizano-Martianez, C. R. Fuerte-Esquivel, and D. Ruiz-Vega, "Global transient stability-constrained optimal power flow using an OMIB reference trajectory," *IEEE Trans. Power Syst.*, vol. 25, no. 1, pp. 392–403, Feb. 2010.

[24] H.-H. Chiang, F. F. Wu, and P. P. Varaiya, "Foundations of the potential energy boundary surface method for power system transient stability analysis," *IEEE Trans. Circuits Syst.*, vol. CS-35, no. 6, pp. 712–728, Jun. 1988.

[25] Q. Huang, R. Huang, W. Hao, J. Tan, R. Fan, and Z. Huang, "Adaptive power system emergency control using deep reinforcement learning," *IEEE Trans. Smart Grid*, vol. 11, no. 2, pp. 1171–1182, Mar. 2020.

[26] Q. Jiang, Y. Wang, and G. Geng, "A parallel reduced-space interior point method with orthogonal collocation for first-swing stability constrained emergency control," *IEEE Trans. Power Syst.*, vol. 29, no. 1, pp. 84–92, Jan. 2014.

[27] Z. Li, G. Yao, G. Geng, and Q. Jiang, "An efficient optimal control method for open-loop transient stability emergency control," *IEEE Trans. Power Syst.*, vol. 32, no. 4, pp. 2704–2713, Jul. 2017.

[28] Z. Li, G. Geng, and Q. Jiang, "Transient stability emergency control using asynchronous parallel mixed-integer pattern search," *IEEE Trans. Smart Grid*, vol. 9, no. 4, pp. 2976–2985, Jul. 2018.

[29] G. Gan, Z. Zhu, G. Geng, and Q. Jiang, "An efficient parallel sequential approach for transient stability emergency control of large-scale power system," *IEEE Trans. Power Syst.*, vol. 33, no. 6, pp. 5854–5864, Nov. 2018.

[30] Y. Ma, G. Geng, Q. Jiang, and R. Yan, "Transient stability emergency control for AC/DC grids considering successive commutation failures," *IET Gener., Transmiss. Distrib.*, vol. 16, no. 7, pp. 1319–1333, Apr. 2022.

[31] S. Robak, J. Machowski, M. M. Skwarski, and A. Smolarczyk, "Transient stability improvement by generator tripping and real-time instability prediction based on local measurements," *IEEE Access*, vol. 9, pp. 130519–130528, 2021.

[32] M. Koaizawa, M. Nakane, K. Omata, and Y. Kokai, "Actual operating experience of on-line transient stability control systems (TSC systems)," in *Proc. IEEE Power Eng. Soc. Winter Meeting. Conf.*, Jan. 2000, pp. 84–89.

[33] F. Milano, *Power System Modelling and Scripting*. New York, NY, USA: Springer, 2010.

[34] M. Dicorato, G. Forte, and M. Trovato, "Wind farm stability analysis in the presence of variable-speed generators," *Energy*, vol. 39, no. 1, pp. 40–47, Mar. 2012.

[35] K. L. Teo and L. S. Jennings, "Nonlinear optimal control problems with continuous state inequality constraints," *J. Optim. Theory Appl.*, vol. 63, no. 1, pp. 1–22, Oct. 1989.

[36] H. Liu, C. Chen, X. Lv, X. Wu, and M. Liu, "Deterministic wind energy forecasting: A review of intelligent predictors and auxiliary methods," *Energy Convers. Manag.*, vol. 195, pp. 328–345, Sep. 2019.

[37] C. J. Goh and K. L. Teo, "Control parametrization: A unified approach to optimal control problems with general constraints," *Automatica*, vol. 24, no. 1, pp. 3–18, Jan. 1988.

[38] S. Mehrotra, "On the implementation of a primal-dual interior point method," *SIAM J. Optim.*, vol. 2, no. 4, pp. 575–601, 1992.

[39] D. F. Shanno, "Conditioning of quasi-Newton methods for function minimization," *Math. Comput.*, vol. 24, no. 111, pp. 647–656, 1970.

[40] P. Kundur, *Power System Stability and Control*. New York, NY, USA: McGraw-Hill, 1994.

[41] A. Haddadi, M. Zhao, I. Kocar, U. Karaagac, K. W. Chan, and E. Farantatos, "Impact of inverter-based resources on negative sequence quantities-based protection elements," *IEEE Trans. Power Del.*, vol. 36, no. 1, pp. 289–298, Feb. 2021.

YUNFEI MA received the B.S. degree in electrical engineering from the College of Electrical Engineering, Shandong University, Jinan, China, in 2017. He is currently pursuing the Ph.D. degree with the College of Electrical Engineering, Zhejiang University, Hangzhou, China.

His research interests include power system stability and control and power system optimization algorithm.

XIN WANG received the B.S. degree in electrical engineering from the College of Electrical Engineering, Chongqing University, Chongqing, China, in 2021. He is currently pursuing the M.S. degree with the College of Electrical Engineering, Zhejiang University, Hangzhou, China.

His research interests include power system transient stability simulation and analysis.

GUANGCHAO GENG (Senior Member, IEEE) received the B.S. and Ph.D. degrees in electrical engineering from the College of Electrical Engineering, Zhejiang University, Hangzhou, China, in 2009 and 2014, respectively.

From 2012 to 2013, he was a Visiting Student with the Department of Electrical and Computer Engineering, Iowa State University, Ames, IA, USA. From 2014 to 2017, he was a Postdoctoral Fellow with the College of Control Science and Engineering, Zhejiang University, and the Department of Electrical and Computer Engineering, University of Alberta, Edmonton, AB, Canada. From 2017 to 2019, he was a Research Assistant Professor with the College of Electrical Engineering, Zhejiang University, where he is currently an Associate Professor. His research interests include power non-intrusive sensing technology, data analytics in power systems, and power system stability and control.

QUANYUAN JIANG (Senior Member, IEEE) received the B.S., M.S., and Ph.D. degrees in electrical engineering from the Huazhong University of Science and Technology, Wuhan, China, in 1997, 2000, and 2003, respectively.

From 2006 to 2008, he was a Visiting Associate Professor with the School of Electrical and Computer Engineering, Cornell University, Ithaca, NY, USA. He is currently a Professor with the College of Electrical Engineering and the Academic Dean of Graduate School, Zhejiang University, Hangzhou, China. His research interests include power system stability and control, applications of energy storage systems, and high performance computing technique in power systems.